Research Article

Dabosmita Paul, Marko Petrič, Miha Humar, Erika Švara Fabjan, Milan Gaff*, and Daniela Tesařová

Enhancing the superhydrophobicity, UV-resistance, and antifungal properties of natural wood surfaces *via in situ* formation of ZnO, TiO_2, and SiO_2 particles

https://doi.org/10.1515/ntrev-2025-0171
received September 3, 2024; accepted April 21, 2025

Abstract: This study investigates the *in situ* synthesis and formation of zinc oxide (ZnO), silicon dioxide (SiO_2), and titanium dioxide (TiO_2) particles within the wood structure to modify the wood surface, aiming to improve the hydrophobicity, UV resistance, and antifungal properties of Scots pine and Norway spruce wood. The formation of particles in the modified wood and untreated wood surfaces was characterised using scanning electron microscopy (SEM) with energy-dispersive X-ray spectroscopy (EDS) to study the microstructure and chemical composition, X-ray diffraction (XRD) to determine the type of crystallisation, and attenuated total reflectance-Fourier transform infrared (ATR-FTIR) spectroscopy to analyse the bonding forces. Results indicated that TiO_2 and SiO_2 treatments significantly improved both wood species' surface hydrophobicity and UV resistance properties compared to ZnO-treated wood. On the other hand, ZnO treatment enhanced antifungal properties, offering effective protection against fungal decay in both wood species, while TiO_2 and SiO_2 showed less pronounced effects. This study showcases the potential of ZnO, SiO_2, and TiO_2 particle treatments to enhance the surface properties of natural wood, paving the way for the effective and environmentally friendly development of hybrid wood for various applications in the wood industry and beyond.

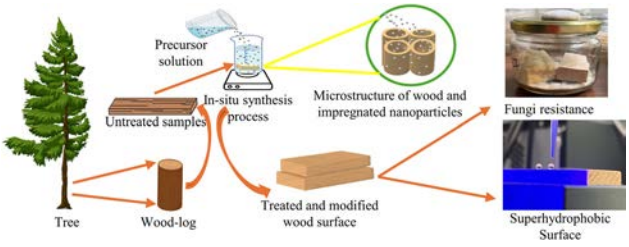

Graphical abstract

Keywords: *in situ* synthesis, hydrophobicity, UV resistance, antifungal properties, surface modification, hybrid wood

*** Corresponding author: Milan Gaff**, Department of Furniture, Design and Habitat (FFWT), Mendel University in Brno, 1, Zemědělská 1665, Černá Pole, Brno-sever, 613 00, Czech Republic; Faculty of Civil Engineering, Experimental Centre, Czech Technical University in Prague, Prague, Czech Republic, e-mail: milan.gaff@mendelu.cz
Dabosmita Paul: Department of Furniture, Design and Habitat (FFWT), Mendel University in Brno, 1, Zemědělská 1665, Černá Pole, Brno-sever, 613 00, Czech Republic, e-mail: dabosmita.paul@mendelu.cz
Marko Petrič: Department of Wood Science and Technology, Biotechnical Faculty, University of Ljubljana, Jamnikarjeva 101, SI-1000 Ljubljana, Slovenia, e-mail: marko.petric@bf.uni-lj.si
Miha Humar: Department of Wood Science and Technology, Biotechnical Faculty, University of Ljubljana, Jamnikarjeva 101, SI-1000 Ljubljana, Slovenia, e-mail: miha.humar@bf.uni-lj.si
Erika Švara Fabjan: Slovenian National Building and Civil Engineering Institute, Dimičeva 12, Ljubljana, SI-1000, Slovenia, e-mail: erika.svara-fabjan@zag.si
Daniela Tesařová: Department of Furniture, Design and Habitat (FFWT), Mendel University in Brno, 1, Zemědělská 1665, Černá Pole, Brno-sever, 613 00, Czech Republic, e-mail: daniela.tesarova@mendelu.cz

1 Introduction

Wood has been valued since ancient times for its unique chemical and physical qualities. Wood's renewable nature and aesthetic qualities make it a highly versatile material for applications in construction, furniture making, pulp energy production, and packaging. However, external factors such as sunlight, rain, temperature fluctuations, insects, and bacterial and fungal decay can affect the wood's physical and chemical properties [1,2]. The porous structure of wood has inherent limitations and vulnerabilities that risk its long-term performance [3,4]. Untreated, non-durable wood has several drawbacks concerning hydrophobicity, susceptibility to ultraviolet (UV) degradation, and vulnerability to fungal infestation, all compromising its performance and endurance [5].

Therefore, enhancing wood's hydrophobic properties helps prevent moisture damage, reducing decay and deformation, thereby improving the durability and extending its service life in furniture, doors, windows, and outdoor structures [6]. Traditional methods like thermal, enzymatic, plasma, and chemical treatments are commonly used to improve wood protection. However, thermal and enzymatic treatments often target specific properties, which may reduce the durability or limit the overall functionality [7,8]. Plasma treatments, while effective at modifying the surface, lack depth and long-term durability and typically require complex procedures [9]. Similarly, conventional chemical modification [10] approaches that involve grafting long-chain alkyl groups onto the wood surface to enhance its natural roughness encounter difficulties in achieving ideal superhydrophobicity [11]. This is particularly challenging in the radial and tangential sections of the wood, where the natural structure lacks the necessary micro- or nanoscale roughness for optimal performance [12]. Consequently, these methods fail to provide durable, effective protection after cutting the wood. In this context, this research focuses on enhancing natural wood for outdoor use by incorporating zinc oxide (ZnO), titanium dioxide (TiO_2), and silicon dioxide (SiO_2) to improve hydrophobicity, UV resistance, and durability through stable inorganic–organic hybrid composites. Organic–inorganic hybrid composites, which combined the advantages of polymers and inorganic compounds, are widely studied for their unique properties and applications in catalysts, coatings, solar cells, and sensors [13–15]. Due to its multifunctionality, hybrid wood material gained popularity among researchers in recent years [10,11]. Studies explored the fabrication and characterisation of magnetic wood [16,17] with nanoparticles, highlighting applications in electromagnetic absorption, heating, and wearable devices using materials like ZnO, CuO, and $CaCO_3$ [18–20].

Incorporating inorganic particles into wood offers a multifaceted approach to enhance its durability and longevity. Particles such as ZnO, SiO_2, and TiO_2 protect wood against environmental factors like moisture, UV radiation, and fungal degradation [21]. With their high surface area and wide bandgap, ZnO particles effectively block UV radiation, safeguarding against discolouration due to lignin degradation [22]. Additionally, their fungicidal properties influence fungal growth [11,19]. SiO_2 particles, known for their thermal stability and dispersibility, contribute to wood protection and find applications in various fields, including drug delivery and surface coatings [23]. However, high concentrations of both ZnO and SiO_2 particles pose respiratory hazards, necessitating caution in handling [24]. TiO_2 particles, renowned for their photocatalytic activity and UV absorption, offer self-cleaning properties and environmental remediation benefits. Despite their safety in topical applications, airborne exposure to TiO_2 particles raises respiratory concerns [25]. Even though there is no regulation for the quantity of particles, a low concentration was used in the respective study to achieve the best results and avoid health hazards. Nevertheless, incorporating these particles into wood presents a comprehensive strategy to enhance its resilience against environmental stresses [26]. Although significant progress has been made in developing wood–inorganic composites, a research gap remains in understanding how different wood species respond to various particle treatments. Most existing studies focus on the functional properties of treated wood but overlook the species-specific structural and chemical interactions with inorganic particles. To address this gap, our study aimed to enhance resistance to fungal degradation while exploring the compatibility of two commonly used gymnosperm species, Scots pine and Norway spruce, with ZnO, TiO_2, and SiO_2 treatments. These species differ in anatomical features such as resin canal presence, parenchyma cell distribution, and grain texture [27], which may influence their interaction with impregnated particles. By comparing treated and untreated samples using scanning electron microscopy coupled with energy-dispersive X-ray spectroscopy (SEM–EDS), X-ray diffraction (XRD), and attenuated total reflectance-Fourier transform infrared (ATR-FTIR) spectroscopy analyses and performance tests for hydrophobicity, UV resistance, and antifungal activity, this research provides new insights into species-specific responses and offers targeted solutions for improving wood durability in outdoor applications.

2 Materials and methods

2.1 Materials

Norway spruce (*Picea abies*) and Scots pine (*Pinus sylvestris*) wood samples were made from trees cultivated in the Czech Republic and Slovakia. These two wood species were chosen, as non-durable conifers like spruce and pine are frequently used in construction applications in Europe. Ethyl alcohol (99%), sodium hydroxide, zinc acetate dihydrate, hexamethylenetetramine (HMTA), hexadecyltrimethoxysilane (HDTMS), zinc nitrate hexahydrate, and acetic acid (99.8%) were bought from Lach:ner. Tetraethyl orthosilicate (TEOS, 98%), titanium(IV) *n*-butoxide (98+%), and ammonium hydroxide (NH_4OH) for analysis (28–30 wt% solution of NH_3 in water) were bought from Thermo Scientific. Distilled water (DW) was used throughout the study. All the chemicals were used without further purification.

2.2 Sample preparation

Pine and spruce wood samples were cut into sizes of (0.5 × 2.0 × 5.0) cm^3 and (1.5 × 2.5 × 5.0) cm^3. Then, the samples were cleaned ultrasonically in deionised water for 15 min and dried in a chamber at 105°C until a constant mass was achieved.

2.3 Preparation of the ZnO-modified wood composite material

ZnO particles in wood were synthesised using zinc acetate dihydrate, sodium hydroxide, and HMTA. Zinc acetate dihydrate was initially dissolved in 200 ml of ethyl alcohol to prepare a 0.05 M solution. The solution was stirred at 60°C in a magnetic stirrer for an hour. Then, dried wood samples were immersed in the solution under a vacuum of 0.01 MPa for 30 min. Afterwards, the samples were left to be soaked at room temperature (23°C) for 2 h. A 0.4 M sodium hydroxide (NaOH) solution was prepared in a separate beaker by dissolving pellets of NaOH in 100 ml of DW. This NaOH solution served as the base for the precipitation reaction. After that, an adequate amount of NaOH solution was added slowly into the solution with the soaked samples, causing the formation of a white precipitate. The samples were left to soak in the solution for 24 h. Afterwards, at 80°C, the samples were dried for approximately 4 h. In the synthesis process, the samples were impregnated with ZnO seeds. The treated samples were used for subsequent ZnO growth under hydrothermal conditions. For that, the seed-coated samples were impregnated with zinc nitrate hexahydrate (0.02 M) and HMTA (0.02 M) solution mixture (1:1 ratio) made with a standard aqueous amount of deionised water for 6 h at 80°C. The resultant wood samples were properly rinsed with deionised water. Finally, the samples were cured at 105°C for 24 h. The hybrid wood of ZnO–wood composite was thus prepared using this procedure.

2.4 Preparation of the TiO_2-modified wood composite material

TiO_2 particles were synthesised using the sol–gel process. A solution of 0.05 M titanium(IV) *n*-butoxide with 200 ml of ethanol and 100 ml of DW formed a homogeneous solution A with continuous stirring. Solution B was prepared by mixing 0.02 M solution of acetic acid and 100 ml of ethanol. Then, solution B was slowly added to solution A at 80°C. The precursor mixture was continuously stirred using a magnetic stirrer for 2 h. Afterwards, the wood samples were immersed in the precursor solution for 30 min in a vacuum chamber at 0.01 MPa. Then, the samples were taken from the vacuum chamber and left in the solution at room temperature (23°C) for 24 h. After soaking, the sample was washed with distilled water (DW) to remove the impurities and dried at 80°C in a heating chamber for 6 h. The TiO_2-impregnated samples were immersed in the ethanol solution of 0.02 M hexadecyltrimethoxysilane (HDTMS) for 1 h at 80°C. Then, the samples were dried at room temperature (23°C) for 2 h. After 2 h, the samples were cured at 105°C for 24 h. The hybrid wood of TiO_2–wood composite was thus prepared using the procedure.

2.5 Preparation of SiO_2-modified wood composite material

The sol–gel method involves the reaction process to produce SiO_2 in wood, using 0.05 M solution of TEOS and 0.02 M solution of NH_4OH. This method included the hydrolysis and condensation of TEOS with NH_4OH as a catalyst. Solution A was prepared by mixing TEOS with 50 ml of ethanol, while solution B was made by combining NH_4OH with 350 ml of ethanol. Solution A was added to solution B slowly dropwise, and then the precursor mixture was continuously stirred at 50°C using a magnetic stirrer for 2 h. The dried wood samples were immersed in the precursor solution for 30 min in a vacuum chamber at 0.01 MPa. Then, the samples were taken from the vacuum chamber and left in the solution at room temperature (23°C) for 24 h. Afterwards, they were retrieved from the solution and vigorously cleaned to remove impurities. The SiO_2-vacuum impregnated wood samples were immersed in 0.02 M solution of HDTMS and 300 ml of ethanol mixture for 1 h at 80°C. Then, the samples were dried at room temperature (23°C) for an hour. After 2 h, the sample was cured at 105°C for 24 h. The hybrid wood of SiO_2–wood composite was thus prepared by this procedure.

2.6 Characterisation and testing methods

Both species' samples were divided into two groups: untreated and treated samples. The samples were characterised by the following procedures: SEM analysis, XRD analysis, determination of water uptake, and antifungal assay. However, for the resistance against UV radiation

and wettability tests, the samples of both species were divided into two parts: in the first part, we measured the difference between treated and untreated samples before exposing them to UV light, and in the second part we measured the difference between the treated and untreated samples after exposing to UV light for 336 h.

2.6.1 SEM analysis

To observe the microstructural characteristics of the materials, the samples were prepared in longitudinal sections for both untreated and treated samples by cutting them with a sharp blade. These sections were then mounted onto conductive carbon tape and coated with a layer of 15 µm thick gold using a sputtering technique. Subsequently, the analysis was performed using a scanning electron microscope (Mira-STAN instrument from Tescan), with an acceleration voltage of 5 kV and a beam current of 10 pA to observe the samples in detail. EDS was carried out using an Oxford Instruments AZtecOne system to analyse the composition and distribution of elements within the samples.

2.6.2 XRD analysis

XRD analyses were performed using an Empyrean diffractometer (PANalytical, The Netherlands) with Cu Kα radiation. Measurements were performed at a tube current of 40 mA and a tube tension of 45 kV, using a 2θ step size of 0.006°, and the measurement time was 120 s per step. Data were collected over a 2θ range of 10° to 70°. The results were analysed using HighScore (PANalytical, The Netherlands) diffraction software.

2.6.3 FTIR analysis

ATR-FTIR spectroscopy was performed with a Bruker Invenio S. The sample and background scans were each conducted 16 times, with data collected in the range of 4,000–400 cm^{-1}. The measurement time was 15 s in transmittance mode. OPUS software was used to analyse the results.

2.6.4 Water uptake tests

A KRUSS Processor Tensiometer K100 was used to carry out short-term water uptake tests under room conditions. The K100 operates by putting the cross-section of samples in contact with the surface of water and precisely measuring the changes in their weight over time due to capillary sorption of water. This enables the determination of water uptake rates and capacity, providing valuable insights into the material's behaviour when exposed to liquid water.

Water uptake tests were carried out with untreated and treated samples of both species. The sample size was (0.5 × 2.0 × 5.0) cm^3. Using equation (1), water uptake was calculated:

$$W = \frac{m}{A}\left[\frac{g}{m^2}\right], \tag{1}$$

where m is the mass of samples and A is the axial surface area of the sample.

During water absorption tests with the KRUSS Processor Tensiometer K100, radial measurements were typically conducted when assessing water uptake perpendicular to the wood grain. Tangential measurements, on the other hand, were carried out when assessing water absorption parallel to the wood grain. These measurements provide insights into how water penetrates wood fibres of different orientations. Our research experimented with transverse parts of each sample.

2.6.5 Colour change

The colour change was measured to determine the influence of particle treatment on the samples as a result of exposure to UV radiation. This is one of the several tests used to assess the UV resistance. UV irradiation was carried out in a UV chamber (OSRAM Ultra-Vitalux 300 W lamp with radiation wavelengths between 315 and 400 nm; self-constructed at the University of Ljubljana). Treated and untreated wood samples, with dimensions of 0.5 × 2.0 × 5.0 cm^3, were arranged at uniform intervals and exposed to fungal cultures for a period of three weeks. The colour of the specimens was measured with a spectrophotometer BYK-Gardner GmbH, Spectro-guide 45/0,6801. According to the CIELAB colour measurement system, L^* represents lightness, a^* represents the green-red axis, and b^* represents the blue-yellow axis. The following equation defines the colour difference:

$$\Delta E^* = \sqrt{(\Delta L^*)^2 + (\Delta a^*)^2 + (\Delta b^*)^2}, \tag{2}$$

where ΔE^* is the colour difference, ΔL^* is the lightness difference, Δa^* is the chroma change from green to red or in the other direction, and Δb^* is the chroma change from blue to yellow or in the other direction.

The symbol Δ represents the differences between samples' initial and final colour parameters after treatment or UV irradiation. L^*, a^*, and b^* denote the average values obtained from three locations on each sample. Five measurements were done for each treated and untreated sample.

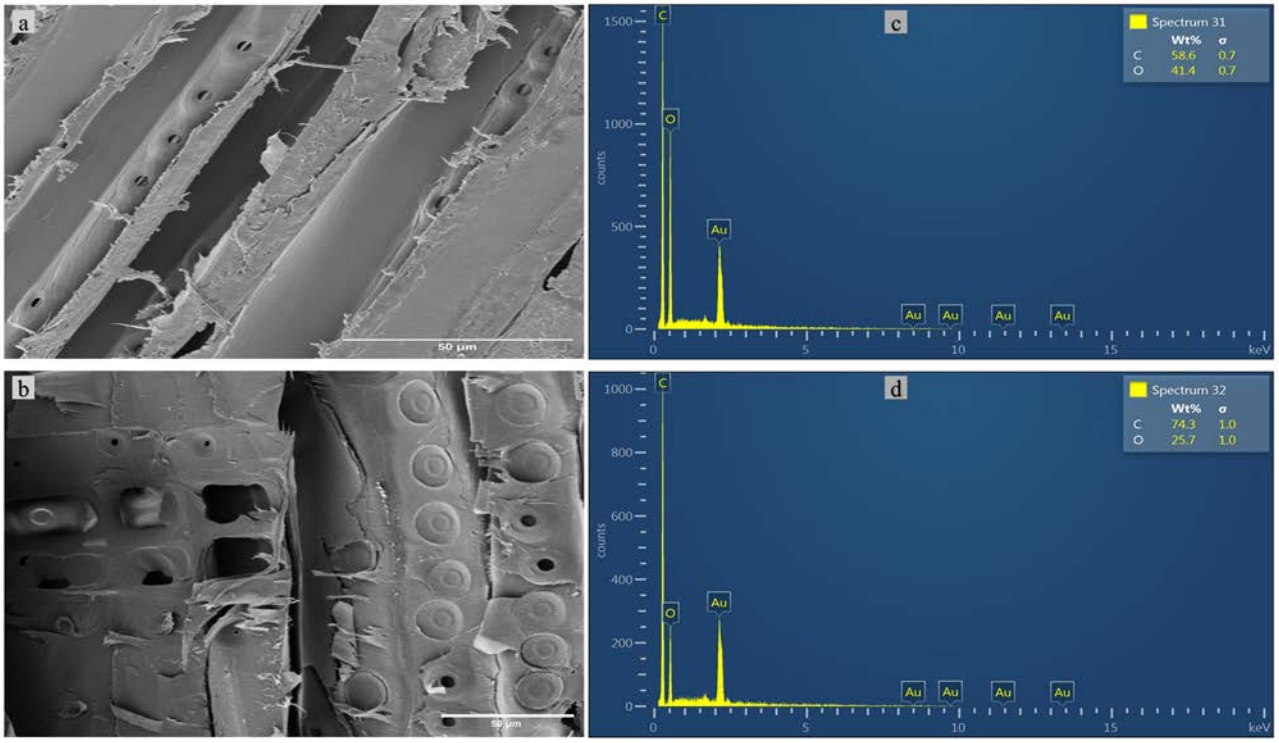

Figure 1: SEM image and EDS micrograph: (a) and (b) spruce and pine surface morphology; (c) and (d) spruce and pine elemental composition.

2.6.6 Contact angle (CA) measurements

The CAs of water were measured with the Biolin Scientific Attension Theta equipment. The wood samples measuring (0.5 × 2.0 × 5.0) cm^3 were used for the test. All samples, both the untreated and treated ones, *i.e.* unexposed and exposed to UV were utilised. DW droplets, each with a volume of 6 µl, were applied to measure the water CA on the wood surfaces. The CA values were recorded at room temperature for 0–60 s after application. Five droplets of DW were used for the CA measurements on the tangential surface of each sample.

2.6.7 Durability test

The treated and untreated samples of pine and spruce (1.5 × 2.5 × 5.0) cm^3 were placed on an autoclave before sterilisation at 121°C until it reached 0.15 MPa pressure. In the meantime, we prepared a nutrient medium for fungi, which was 2 l of water and 78 g Difco™ potato dextrose agar. After that, the jars for the experiment were prepared with a mixture of 55 ml for each. Then, they were autoclaved for sterilisation at 121°C until they reached 0.15 MPa pressure. After that, steam-sterilised treated and non-treated specimens were exposed to brown rot fungus (EN113) – *Gloeophyllum trabeum* (Pers.) Murrill (ZIM L018) [28] – for 20 weeks according to the modified Bravery procedure (1996) [29]. The experiment was performed with five replicate specimens per treatment.

2.7 Statistical analysis

After verifying the normality assumption and homogeneity of variance in the data, a one-way analysis of variance (ANOVA) was done to measure the impact of different treatments on fungal mass loss. Following ANOVA, Tukey's method was applied for *post-hoc* comparisons to identify significant differences between specific treatment pairs in the antifungal test.

3 Results and discussion

3.1 Morphology analysis

The structural modifications of wood samples before and after treatments with ZnO, TiO_2, and SiO_2 were analysed by SEM and EDS. The analysed images present longitudinal part of the samples. The analysis was performed to

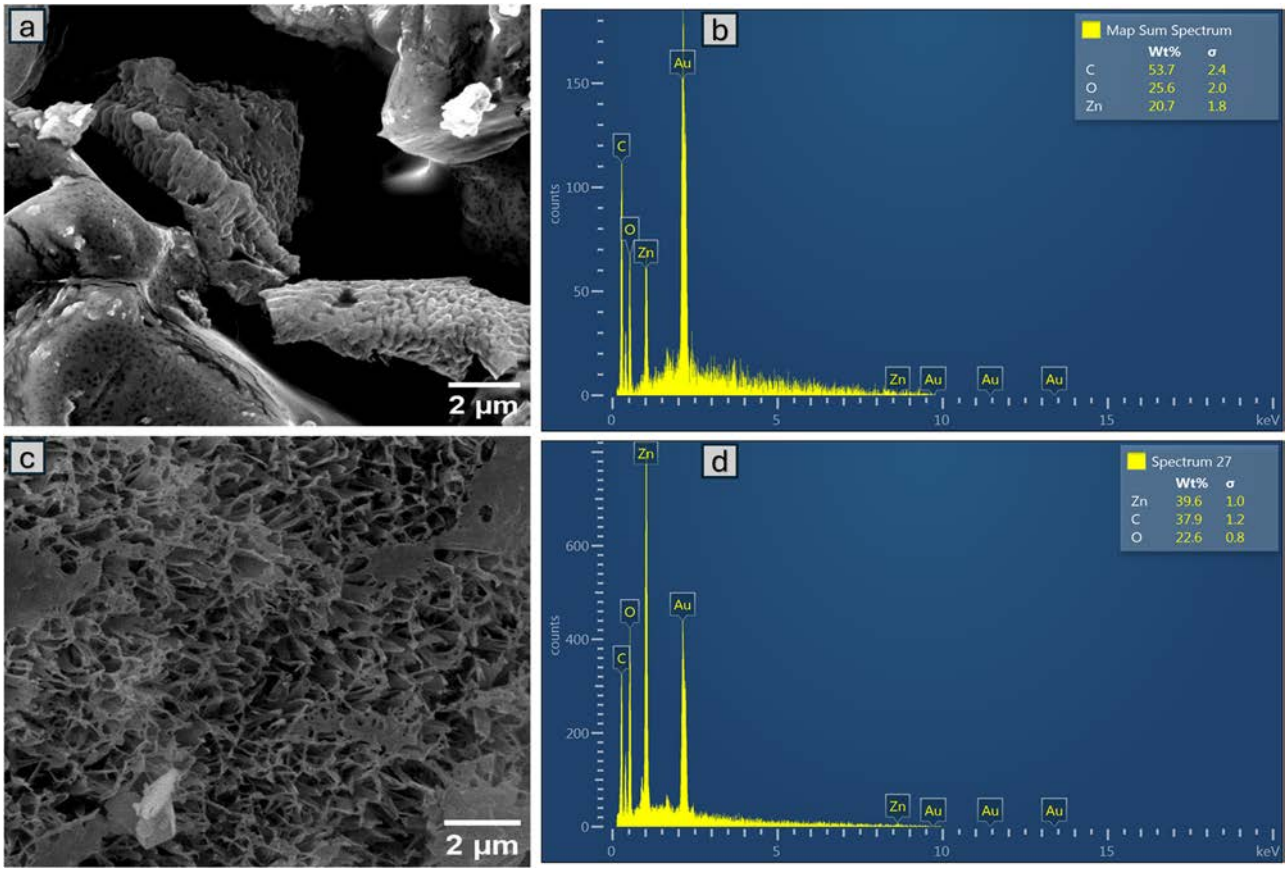

Figure 2: ZnO-treated samples: SEM images of spruce (a) and pine (c); EDS micrographs with a composition ratio of spruce (b) and pine (d).

understand the morphology and composition of the treated and untreated samples [12].

From the SEM analysis (Figure 1(a) and (b)), a smooth cell wall was observed for spruce and pine untreated (control) samples. From the EDS micrographs (Figure 1(c) and (d)), it was observed that only carbon and oxygen elements were present along with peaks for gold as the samples were gold coated for better resolution [30].

In Figure 2(a), from SEM analysis, it was observed that ZnO particles in spruce wood cells tend to aggregate into clusters, forming a layer on the cell wall surface. In contrast, in pine wood samples, ZnO exhibited a flower petal-like configuration (Figure 2(c)). Figure 2(b) and (d) displays the EDS micrographs of Zn composition in spruce and pine samples. The micrographs reveal Zn peaks, along with those of carbon (C), oxygen (O), and the conductive gold (Au) coating. The Zn content was measured as 20.7% in spruce and 22.6% in pine.

SEM analysis of TiO_2-modified hybrid wood samples revealed that TiO_2 particles exhibit a spherical morphology, forming nano- and microparticle clusters across the cell walls of both spruce and pine, as shown in Figure 3(a) and (c). EDS micrographs in Figure 3(b) and (d) display prominent peaks for titanium (Ti), along with carbon (C), oxygen (O), and gold (Au) coating, confirming the presence of Ti-based compounds in the analysed regions. The Ti content was measured as 24.9% in spruce and 24.0% in pine.

The SEM analysis of SiO_2-modified wood samples, shown in Figure 4(a) and (c), revealed that the SiO_2 particles formed small, porous spheres clustered among the fibres and distributed along the cell walls. The EDS micrographs in Figure 4(b) and (d) display prominent peaks for silicon (Si), along with carbon (C), oxygen (O), and conductive gold (Au) coating. Si content was measured as 28.2% in spruce and 13.8% in pine, as depicted in Figure 4(d), with distribution mapping confirming the presence of Si.

The EDS analysis of modified spruce and pine samples with ZnO, TiO_2, and SiO_2 revealed distinct distribution patterns, as shown in Figure 5(a–f). ZnO, present in Figure 5(a) and (b), was uniformly distributed in both wood types, with the Zn $L\alpha_{1\_2}$ emission line being the key to identifying the presence of Zn. This line results from electronic transitions in Zn, where electrons drop from the L-shell to the K-

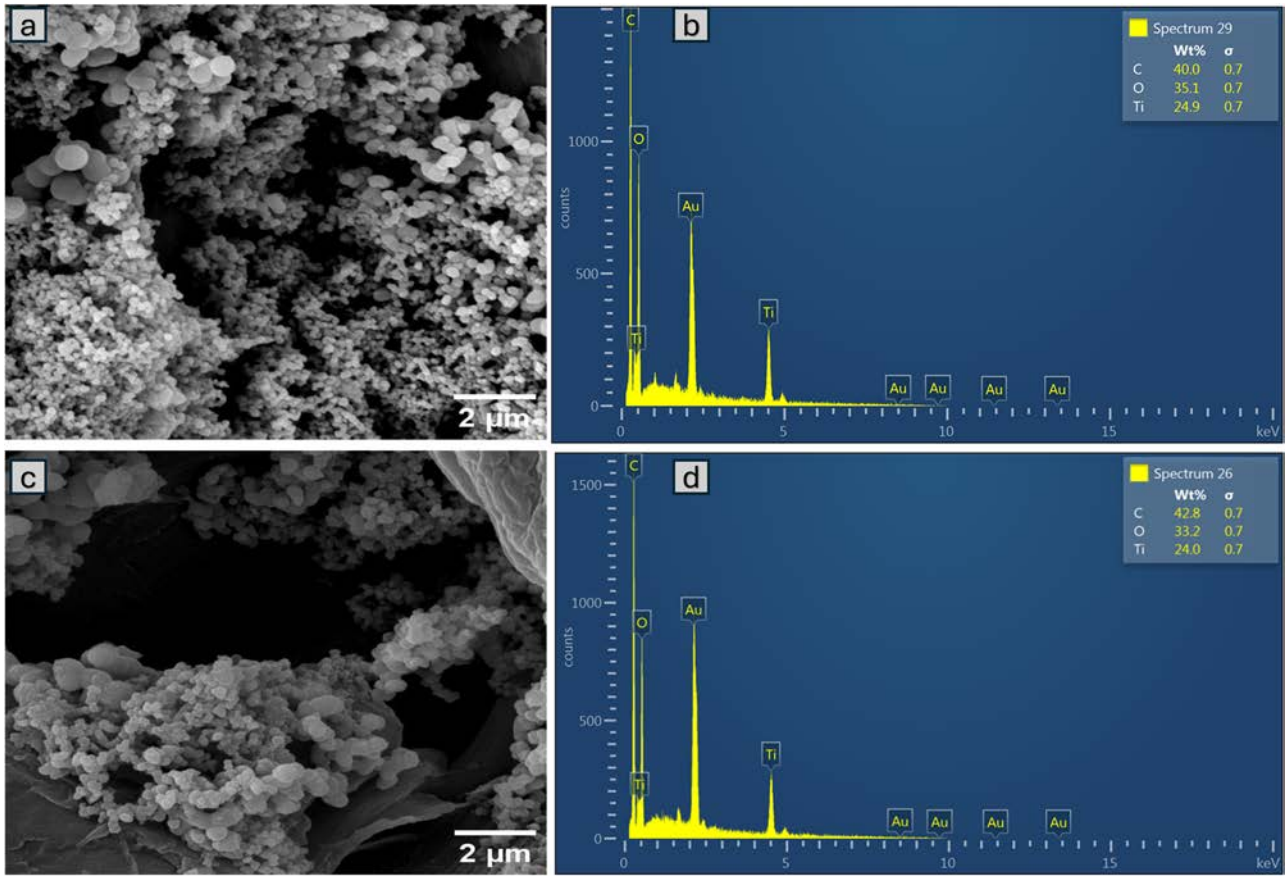

Figure 3: TiO_2-treated samples: SEM images of spruce (a) and pine (c); EDS micrographs with a composition ratio of spruce (b) and pine (d).

shell, with the subscript 1_2 indicating fine spectral splitting due to spin–orbit coupling. The Ti Kα1 line, associated with Ti from TiO_2 (Figure 5(c) and (d)), revealed localised clusters, showing that TiO_2 adhered to specific areas within the wood's cellular framework. The characteristic X-ray emission lines Zn $L\alpha_{12}$, Ti $K\alpha_1$, and Si $K\alpha_1$ confirmed and visualised the distribution of ZnO, TiO_2, and SiO_2, respectively, providing insights into their interactions within the wood matrix. For SiO_2, Figure 5(e) and (f), the Si $K\alpha_1$ line revealed a mixed distribution, with some regions showing concentrated silica deposits and others a more uniform dispersion, highlighting the distinct interaction mechanisms of each modification.

Previous research using SEM analysis demonstrated the successful and uniform deposition of ZnO nanorods on wood surfaces, significantly enhancing the UV resistance, photostability, and overall durability of wood coatings for outdoor use [31,32]. Similarly, another study revealed that densely packed, well-aligned ZnO nanorod arrays provided uniform coverage, leading to remarkable superamphiphobic performance and superior ultraviolet resistance [33]. Additionally, the accumulation of ZnO, TiO_2, and SiO_2 was found to enhance the surface roughness, improving the dimensional stability of the wood. In contrast, our research highlights the formation of ZnO, TiO_2, and SiO_2 particle cluster structures in the cell wall of the samples, which impart superhydrophobicity, UV resistance, and antifungal properties, showcasing distinct multifunctional enhancement.

3.2 Structural analysis

The XRD patterns of untreated and treated spruce and pine samples are presented in Figures 6 and 7, respectively. XRD patterns of both untreated and all treated samples showed broad diffraction peaks at 2θ values of approximately 16.5°, 22.4°, and 35.5°, assigned to cellulose reflections, which usually confirmed the wood samples [34,35]. In the XRD patterns of treated spruce and pine samples using TiO_2 or SiO_2 precursors, namely S_S, S_T, P_S, and P_S samples, as shown in Figures 6 and 7, no additional diffraction peaks were not confirmed in the XRD patterns compared to the untreated samples. The XRD patterns of spruce samples

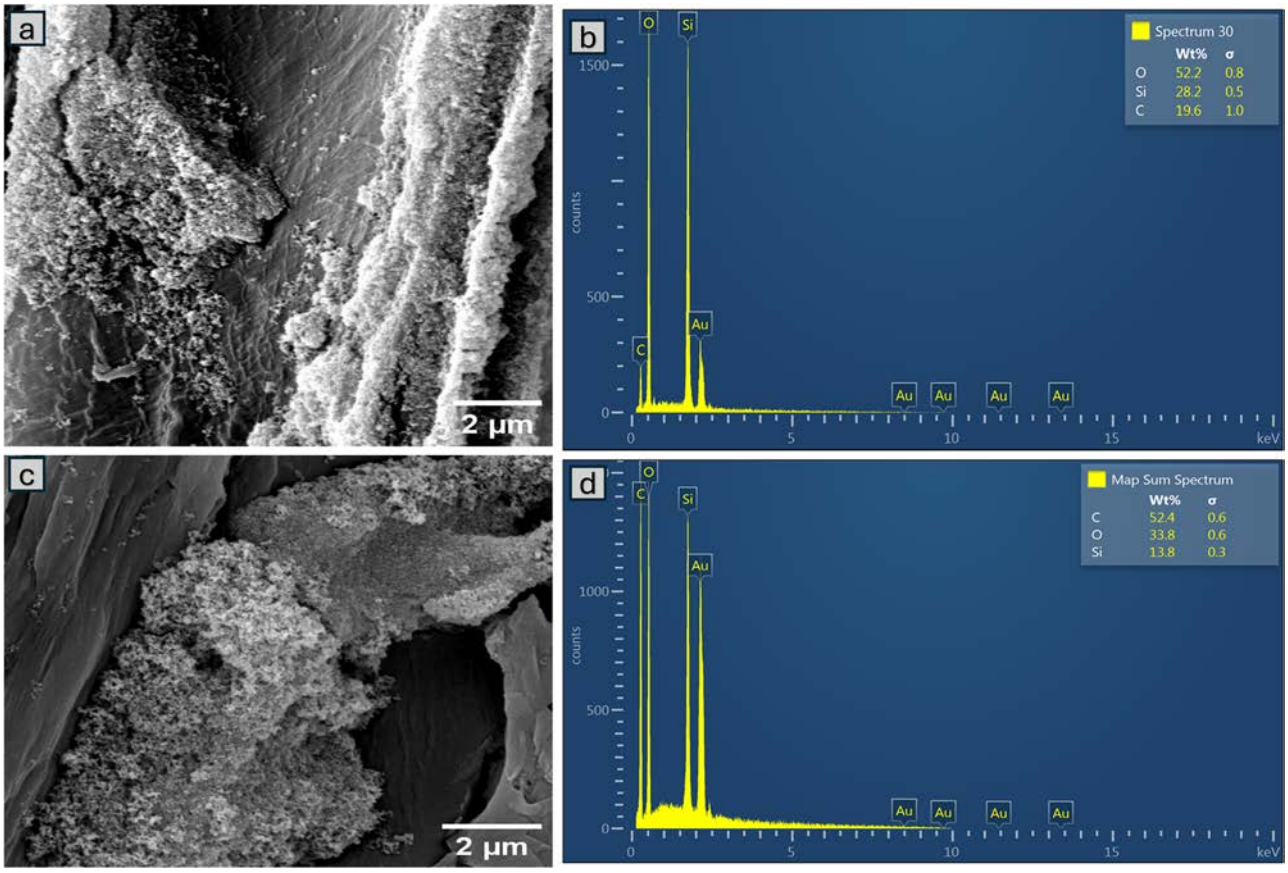

Figure 4: SiO_2-treated samples: SEM images of spruce (a) and pine (c); EDS micrographs with a composition ratio of spruce (b) and pine (d).

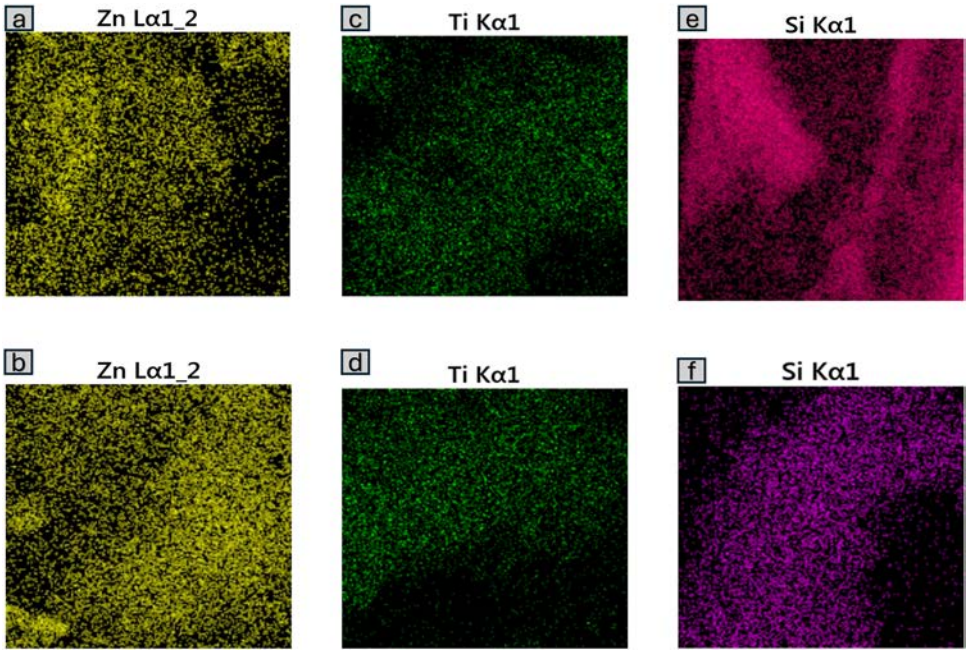

Figure 5: Distribution mapping in spruce and pine for Zn element (a) and (b), Ti element (c) and (d), and Si element (e) and (f).

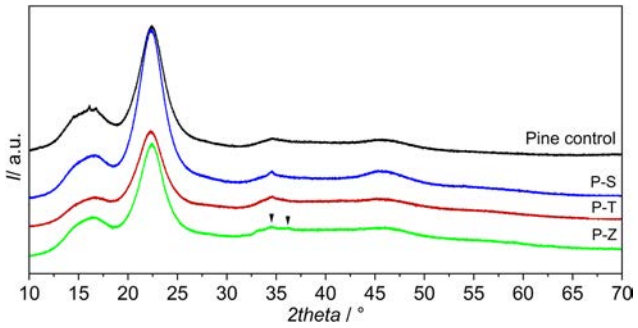

Figure 6: XRD patterns of treated and untreated (control) spruce wood samples.

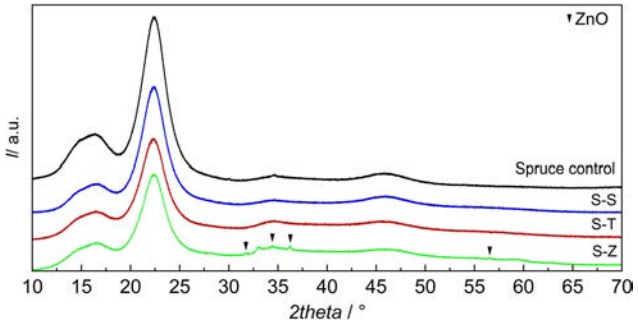

Figure 7: XRD patterns of treated and untreated (control) pine wood samples.

treated using the ZnO precursor showed diffraction peaks at 2θ values of 31.6°, 34.4°, 36.3°, and 56.7° (S_Z, Figure 6) corresponding to the (100), (002), (101), and (110) reflections, respectively, of the crystalline ZnO form described by the ICSD card No. 01-078-2585, which was an indication of the formation of crystalline ZnO in the S_Z sample. In contrast, the XRD patterns of the pine sample treated using ZnO precursor (P_Z in Figure 7) show less defined reflections at 2θ values of approximately 34.4° and 36.3°, suggesting that some crystalline phase was formed. Due to the lack of additional diffraction peaks, the crystalline ZnO could not be confirmed in this sample.

The results did not show any clear crystalline phases of TiO_2 and SiO_2, but in the EDS spectra, it was observed that both elements are present in the samples of both species. Thus, it can be assumed that the particles of TiO_2 and SiO_2 are in the amorphous phase [36–38]. From the previous study, it is notable that although XRD effectively identifies the crystalline phase, EDS assesses the complete elemental composition, capturing both crystalline and amorphous materials [39]. For further confirmation of the elemental compositions, FTIR analysis was made.

3.3 FTIR analysis

FTIR spectra were acquired from the wood surface before and after treatment with three distinct types of particles: TiO_2, SiO_2, and ZnO. Interestingly, the changes observed in the spectra were remarkably similar across all particle treatments. Therefore, we proceeded to analyse them collectively. This analysis is depicted in Figures 8 and 9.

The peak corresponding to the stretching vibration of hydroxyl groups –OH was observed at wavenumber

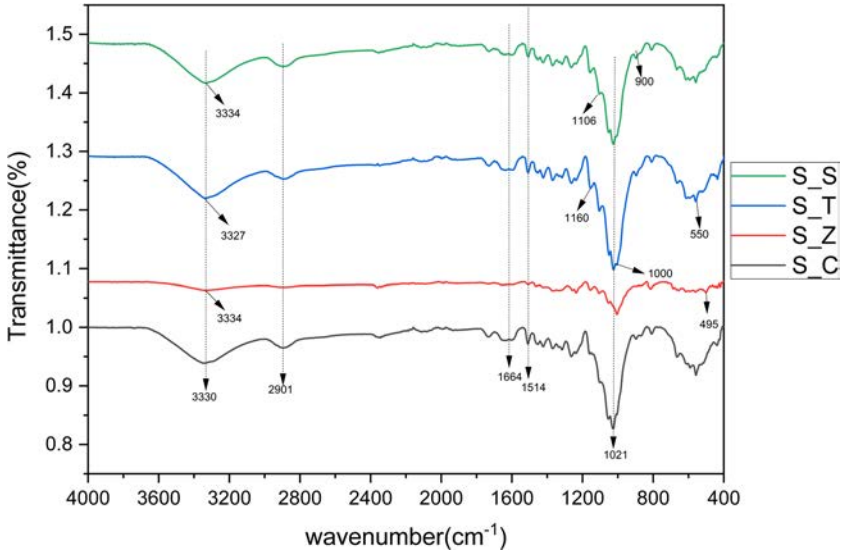

Figure 8: FTIR spectra of treated and untreated (control) spruce wood samples.

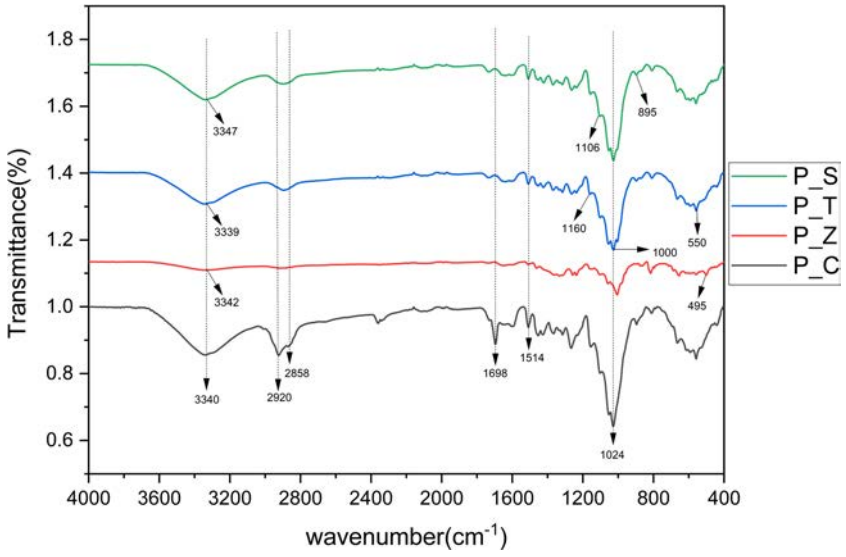

Figure 9: FTIR spectra of treated and untreated (control) pine wood samples.

3,340 cm^{-1} in untreated pine samples (P_C), while it was observed at 3,330 cm^{-1} in untreated spruce samples (S_C). It was noted that the O–H stretching vibrations shifted in all treated samples of both species. The bands at 2,920 and 2,858 cm^{-1}, corresponding to asymmetric CH_3 and symmetric CH_2 stretching vibrations, respectively, were found in the pine control (P_C) samples [40]. In contrast, a 2,901 cm^{-1} band, attributed to C–H stretching vibration, was observed in spruce control (S_C). The C═C bond (lignin and aromatic compound) was not detected in P_C but was present in S_C at 1,664 cm^{-1}. In untreated pine, the C–O–C (cellulose) bond appeared at 1,024 cm^{-1}, whereas in untreated spruce the C–O bond was observed at 1,021 cm^{-1}.

Pine treated and modified with ZnO (P_Z) and spruce treated with ZnO (S_Z) typically confirmed characteristic absorption peaks in the range of 400–600 cm^{-1}, corresponding to the stretching vibrations of Zn–O bonds. Therefore, it was assumed that the absorption peak at

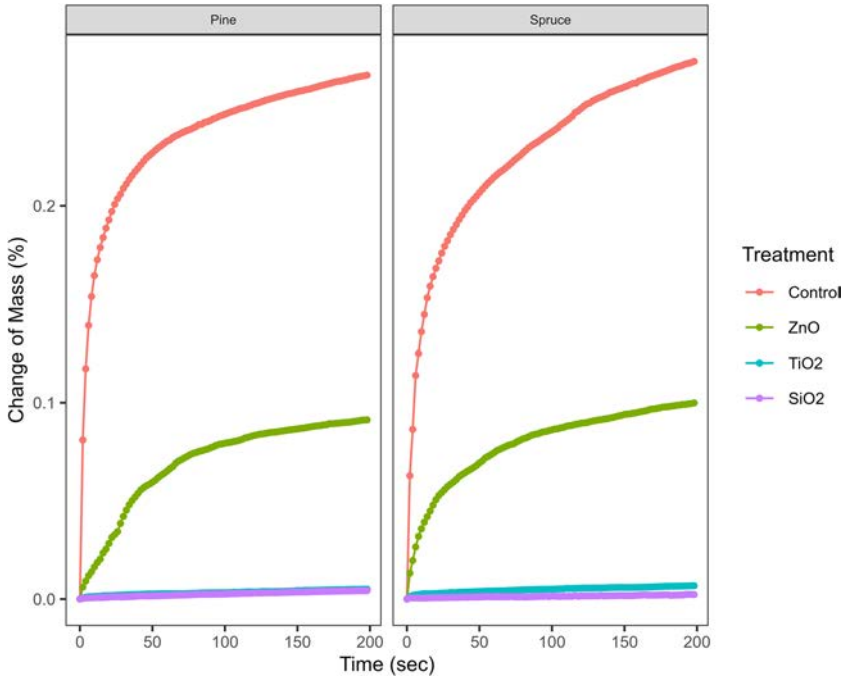

Figure 10: Water uptake of untreated (control) and treated wood samples of pine (left part) and spruce (right part).

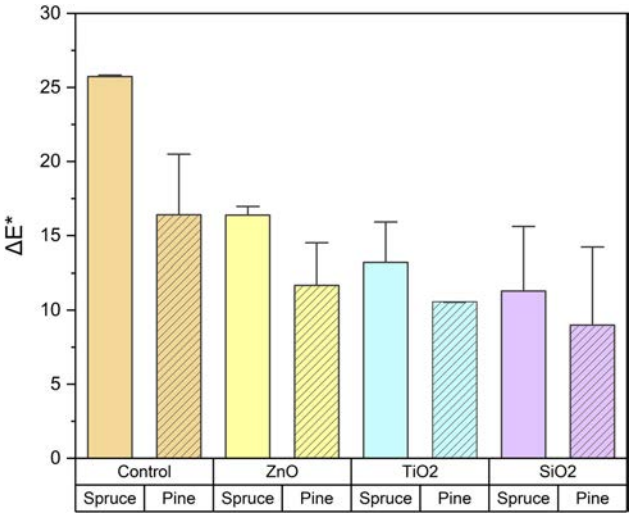

Figure 11: Colour changes showing the difference between untreated and treated samples due to UV exposure. Deviation plots present the standard deviation.

495 cm^{-1} was consistent with the known vibrational modes of ZnO, specifically related to the stretching of Zn–O bonds observed in both modified wood species. The bands below 1,000 cm^{-1} were attributed to Ti–O stretching vibrations characteristic of TiO_2. Peaks at 1,160 and 1,120 cm^{-1} were associated with Ti–O–C bonds, and it was assumed that these peaks resulted from the reaction between Ti–OH and wood –OH in pine (P_T) and spruce (S_T) [41,42]. Around 1,080–1,100 cm^{-1}, the most intense and broad peak corresponding to the asymmetric stretching vibrations of the Si–O–Si bond of SiO_2 was observed. A strong band around 1,106 cm^{-1} [40,43] attributed to the asymmetric stretching vibrations of the Si–O–Si bonds and a weaker band around 900 cm^{-1} associated with the symmetric stretching vibrations of the Si–O–Si bonds were observed in both modified wood pine (P_S) and spruce (S_S) [44].

From Table 1, it can be observed that ZnO, TiO_2, and SiO_2 particles demonstrated effective nucleation within the cellulose fibres, initiating growth processes upon immersion of the wood samples in a reaction solution. This reaction solution contained precursors of ZnO, TiO_2, and SiO_2, which interacted with the wood surface through hydrogen bonds, a process augmented by hydrothermal energy [45]. Differences in deposition between spruce and pine were observed, attributed primarily to variations in their hydroxyl group compositions, which facilitated the adherence of particles to the wood's −OH groups [46]. Such bonding notably enhanced the stability and durability of the deposition [42].

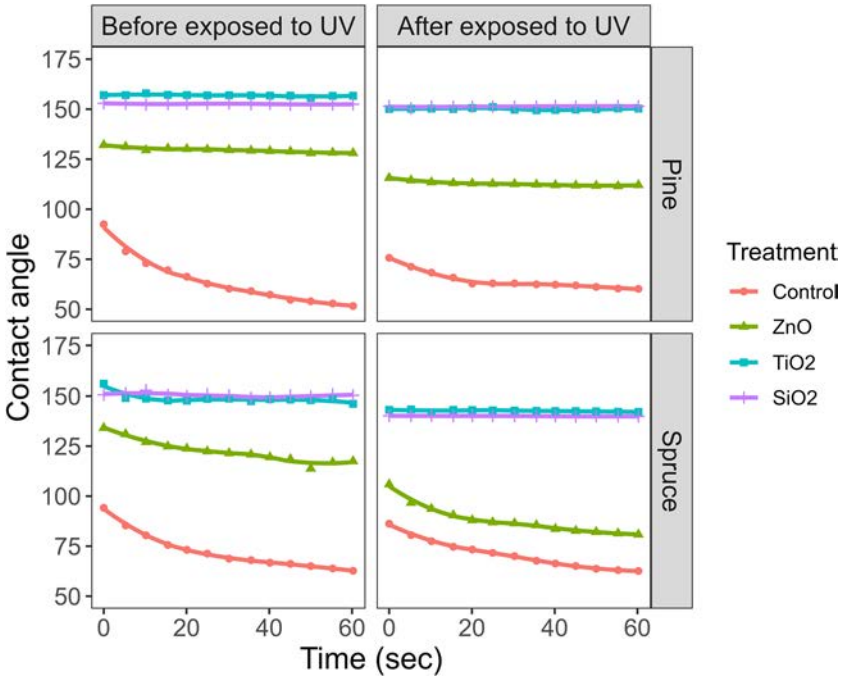

Figure 12: (Top left corner) CAs of the untreated (control) and treated pine wood samples before UV exposure and (top right corner) CAs of these samples after UV exposure. (Bottom left and right corners) CAs of the untreated (control) and treated pine wood before and after UV exposure, respectively.

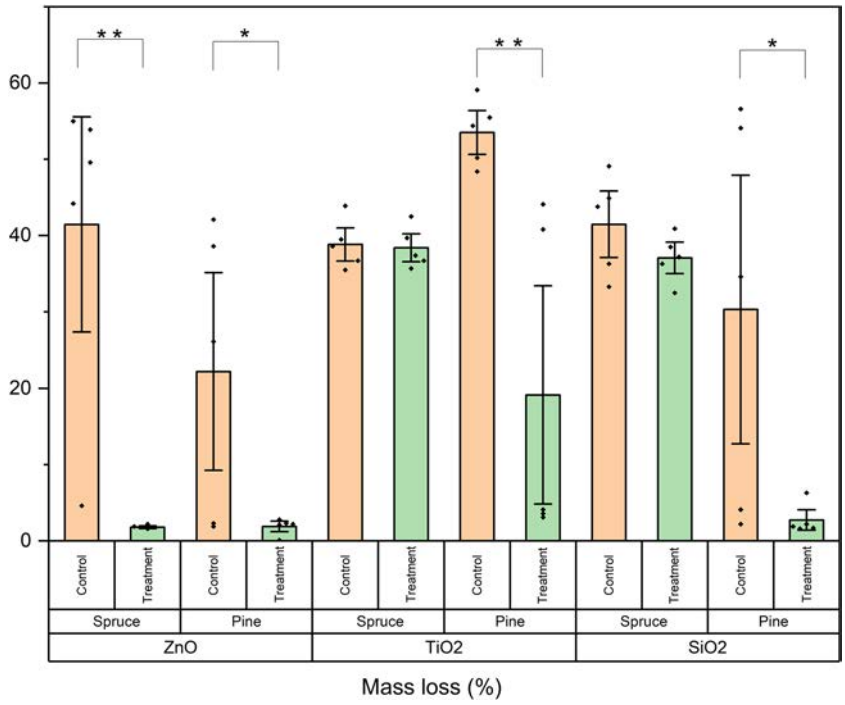

Figure 13: Mass loss of untreated (control) and ZnO, SiO_2, and TiO_2 treated wood of pine and spruce after exposure to the fungus. Significance codes: $p < 0.001$(**); $p < 0.05$(*).

3.4 Water uptake testing

Water uptake testing revealed that the treatments effectively reduced water absorption across both species of wood samples, demonstrated by absorption rates over time. The methodology involved submerging the cross-sections of treated and untreated samples in water, with measurements conducted using a tensiometer to assess water uptake across the grain. For each sample, no repetition has been done. According to the findings in Figure 10, treated samples with TiO_2 and SiO_2 particles exhibited superior water repellence compared to those with ZnO particles and control samples in both wood species. Moreover, the literature suggests that particle coating with the

Table 1: Description of FTIR peaks and their corresponding group

Wavenumber (cm^{-1})	Functional group/bond	Samples	Description
3,340	–OH (hydroxyl group)	P_C	Stretching vibration in untreated pine
3,330	–OH (hydroxyl group)	S_C	Stretching vibration in untreated spruce
2,920	CH_3 (asymmetric stretching)	P_C	Present in pine control
2,858	CH_2 (symmetric stretching)	P_C	Present in pine control
2,901	C–H (stretching vibration)	S_C	Observed in spruce control
1,664	C═C (lignin and aromatic compounds)	S_C	Present in untreated spruce; not detected in untreated pine
1,024	C–O–C (cellulose)	P_C	Observed in untreated spruce
1,021	C–O	S_C	Observed in untreated spruce
495	Zn–O	P_Z	Stretching vibrations of Zn–O bonds in ZnO-treated
400–600	Zn–O	P_Z, S_Z	Characteristic absorption peak range for ZnO
Below 1,000	Ti–O	P_T, S_T	TiO_2 stretching vibration characteristic
1,160	Ti–O–C	P_T	Reaction product of Ti–OH and wood–OH in pine
1,120	Ti–O–C	S_T	Reaction product of Ti–OH and wood–OH in spruce
1,080–1,100	Si–O–Si (asymmetric stretching)	P_S, S_S	Intense broad peak for SiO_2
1,106	Si–O–Si (asymmetric stretching)	P_S, S_S	Strong band for SiO_2
900	Si–O–Si (symmetric stretching)	P_S, S_S	Weaker band for SiO_2

HDTMS saline group enhances superhydrophobic properties, contributing to the observed effects [47]. The treated pine samples displayed marginally higher hydrophobicity than spruce, consistent with prior studies indicating species-specific variations in response to hydrophobic treatments. The decreased water absorption observed with SiO_2 and TiO_2 treatments compared to ZnO treatment was particularly noteworthy, indicating substantial adhesion of hydrophobic metal oxide and particles to the wood cell walls [48]. This adherence hindered water access to cell lumens in the treated wood samples [30,49], leading to a diminished water uptake capacity. Furthermore, these particles increasingly obstructed pits and micropores within the cell wall [50]. Therefore, the water uptake results are consistent with the morphology studies.

3.5 UV resistance analysis

The measurements of colour change were conducted to assess the UV resistance stability of both treated and untreated samples on the surface of pine and spruce woods. The results show the difference of colour in the surface of the samples before and after UV irradiation of 504 h (Table 2 and Figure 11). A positive Δb^* value indicates that the surface of the sample exposed to UV radiation became yellowish. Δa^* in a positive direction means a shift towards reddish tones [36,51]. Compared to the untreated samples, these changes were less pronounced in the treated samples. Also, the overall colour difference (ΔE^*) was lower after UV irradiation of the treated wood sample surface than in the untreated ones for each treatment. The improved UV resistance in the treated samples was observed due to the UV absorption properties of ZnO, TiO_2, and SiO_2 [51]. This result aligns with the findings of previous studies by Sun *et al.*, Rassam *et al.*, and Temiz *et al.* [52–54].

Table 2: Difference in chromatic coordinates between treated and untreated samples before and after UV exposure

Samples	ΔL^*	Δa^*	Δb^*
Control spruce	−17.40 (±3.82)	10.35 (±1.29)	17.23 (±2.37)
Control pine	−14.16 (±3.67)	7.15 (±1.25)	8.62 (±3.09)
ZnO treated spruce	−9.95 (±3.26)	8.16 (±1.84)	11.15 (±1.76)
ZnO treated pine	−7.47 (±1.64)	5.27 (±1.39)	7.77 (±2.61)
TiO_2 treated spruce	−7.93 (±2.63)	6.42 (±1.09)	9.20 (±2.73)
TiO_2 treated pine	−11.75 (±3.87)	3.96 (±3.42)	3.55 (±1.00)
SiO_2 treated spruce	−6.78 (±3.76)	4.17 (±2.02)	7.81 (±5.19)
SiO_2 treated pine	−7.31 (±4.50)	4.52 (±3.26)	5.49 (±4.23)

The values are obtained by comparing the samples' L^*, a^*, and b^* before and after UV exposure for both pine and spruce. Standard deviation values are provided in brackets.

UV radiation significantly impacts lignin in wood, leading to photodegradation, characterised by molecular breakdown and free radical formation [55,56]. Furthermore, SiO_2-treated samples, in terms of colour difference, exhibit better prevention against UV than both TiO_2 and ZnO treated samples. Si impregnation enhances UV resistance by forming a protective barrier that prevents UV penetration, stabilising the wood's structure and increasing its hydrophobicity [57].

3.6 Hydrophobicity

The water CA measurements were conducted on both untreated and treated samples of spruce and pine, as well as after their exposure to UV radiation, as explained in Figure 12. Initially, the untreated (control) samples of both species exhibited hydrophilic properties, which also remained after UV irradiation. Specifically, before UV exposure, the initial CA was approximately 94° for spruce and 92° for pine. After exposure to UV radiation, the initial CA decreased to approximately 86° for spruce and 75° for pine. However, the treated spruce samples over time exhibited CAs ranging from approximately 134° to 117° for ZnO, from 156° to 146° for TiO_2, and ~150° for SiO_2. After exposure to UV light, these values showed negligible changes, with the values of CAs from about 105° to 80° for ZnO, from 143° to 142° for TiO_2, and from 140° to 139° for SiO_2 in spruce. In pine, the CAs before UV exposure were approximately 132° to 128° for ZnO, 157° to 156° for TiO_2, and 152° for SiO_2. Following UV exposure, the values slightly decreased, approximately from 115° to 112° for ZnO, 150° for TiO_2, and from 151° to 141° for SiO_2. The results showed that the treated samples remained hydrophobic even after UV exposure, with minimal changes observed. Particle formation on the sample surface caused increased roughness, as seen in SEM images. This roughness contributed to the CA results, demonstrating the lotus leaf effect and aligning with Cassie–Baxter theory [58] as treated samples of both species' CAs were approximately ≤150° due to the presence of an air pocket on the surface of the treated hybrid wood [43]. The decrease in the water CA in wood due to UV radiation was primarily due to the photodegradation of lignin, which was highly sensitive to UV exposure. It was found in a previous study that UV exposure leads to the breakdown of lignin molecules and the formation of

Table 3: Calculation of both the solid area fraction (f_s) and the air area fraction (f_a)

Wood type	Particles	CA (°)	f_s	f_a
Spruce	ZnO	134	0.328	0.672
Spruce	TiO_2	156	0.093	0.907
Spruce	SiO_2	150	0.144	0.856
Pine	ZnO	132	0.343	0.657
Pine	TiO_2	157	0.082	0.918
Pine	SiO_2	152	0.121	0.879

new, hydrophilic functional groups such as carbonyl and carboxyl. These changes increase the hydrophilicity of the wood's surface, reducing the water CA and enhancing the surface wettability [59]. Therefore, the results in Figure 9 indicate that the treatments decreased lignin degradation on wood surfaces due to UV irradiation while providing UV resistance.

To gain deeper insights into the superhydrophobic characteristics of the treated wood surface, Cassie's equation was utilised. This equation was commonly used for surfaces with heterogeneous roughness and low surface energy, characteristics often associated with superhydrophobicity. In this context, f (equation (3)) represents the fraction of the solid surface in contact with the liquid, while $(1 - f)$ was the fraction of air in contact with the liquid at the surface. θ_C and θ denote the water CAs on the rough surface and smooth surface, respectively. Cassie's equation was used to calculate the fraction of air pockets at the surface of superhydrophobicity [43,60]:

$$\mathrm{Cos}\theta_C = f(\mathrm{Cos}\theta + 1) - 1. \quad (3)$$

In this study, the water CA θ_C on the spruce wood surface treated with particles was approximately 134° for ZnO, 156° for TiO_2, and 150° for SiO_2. For pine wood, the CAs were approximately 132° for ZnO, 157° TiO_2, and 152° for SiO_2. The water CA (θ) of smooth, untreated wood surface was approximately 94° for spruce and 92° for pine. Using Cassie's equation, we calculated the fraction of air in contact with the liquid at the surface. To determine the air area fraction (f_a), we used the fact that the sum of the solid area fraction (f_s) and the air area fraction f_a is equal to 1 in equation (4) [61] (Table 3):

$$f_a = (1 - f_s). \quad (4)$$

Figure 14: Fungi resistance experiment images of treated and untreated wood.

The f_s value represents the fraction of the solid surface area in contact with the liquid, and the f_a value represents the fraction of the surface area that is in contact with air. Furthermore, the study investigated the environmental stability and durability of the superhydrophobic hybrid wood surface. The samples were stored in air for a minimum of 6 months, during which the water CA of the wood surface remained stable without notable changes, demonstrating excellent durability under atmospheric conditions. Images are provided in the supplementary (Figures S1 and S2).

3.7 Fungicidal properties

The results depicted in Figure 13 demonstrate the performance of the treated wood samples against the fungi compared to untreated ones. Specifically, wood samples treated with ZnO, SiO_2, and TiO_2 solutions exhibited clear inhibition zones, indicating inherent antifungal characteristics in both species. Notably, this effect was found to be species-specific. In spruce, significant improvement in antimicrobial properties was observed with ZnO treatment, whereas changes with TiO_2 and SiO_2 treatments were less evident. Conversely, significant changes were observed in pine across all three treatments, with ZnO showing the highest efficacy. The notable increase in mass for both species with ZnO treatment suggests the fundamental role of ZnO in enhancing the composite's antifungal efficacy [62].

Based on the mass losses, the wood can be classified into durability classes (EN 350) [63]. Spruce and pine wood treated with TiO_2 and spruce wood treated with SiO_2 can be classified into the group of the least durable wood-based materials (Durability class 5), while wood species treated with ZnO and pine wood treated with SiO_2 can be classified as very durable (Durability class 1). The difference between the durability of SiO_2-treated pine and spruce can likely be attributed to the permeability difference [64]. Pine sapwood was more permeable than spruce wood; thus, there are likely higher retentions of SiO_2 in pine wood. On the other hand, the fungicidal properties of Zn are well known, resulting in the high durability of treated wood [65] (Figure 14).

4 Conclusions

This study highlights the effectiveness of *in situ* synthesis techniques using inorganic and metal oxide particles in enhancing various wood properties. SEM, EDS, and FTIR analyses confirmed the successful incorporation of ZnO, TiO_2, and SiO_2 into the wood structure, resulting in hybrid wood. Although XRD results were not clearly visible due to the non-destructive nature of the tests, the treatment processes reduced the porosity and increased the surface roughness, leading to enhanced water repellence in the TiO_2- and SiO_2-treated samples compared to the ZnO-treated samples. Among these, SiO_2-modified wood exhibited the best UV resistance, with minimal colour change. The CA of TiO_2- and SiO_2-treated wood remained stable after UV exposure, while ZnO-treated samples showed significant alterations. All treatments improved antifungal properties, with ZnO showing the most pronounced antimicrobial effects, particularly in spruce. Pine also showed improvements with all treatments, with ZnO being the most effective.

Overall, SiO_2-modified pine wood demonstrated superior water repellency, UV resistance, and antifungal protection, while TiO_2 provided exceptional superhydrophobicity and UV resistance. ZnO-treated wood was the most effective in providing antifungal protection for both wood species. These enhancements in hydrophobicity, UV resistance, and antifungal properties contributed to the wood's overall durability, offering internal and surface protection against fungi and water damage, ensuring longevity even when used for furniture or outdoor applications, and reducing maintenance requirements in humid environments.

Further research is needed to understand how these improvements work fully and refine the synthesis process for practical applications across diverse sectors, including the wood industry, electronics, and energy storage.

Acknowledgments: Research programme P2-0273 from Slovenian Research Agency. We acknowledge CzechNanoLab Research Infrastructure supported by MEYS CR (LM2023051).

Funding information: This research was supported by the Internal Grant Agency for Individual Projects at Mendel University in Brno. The specific project number associated with this support is IGA-FFWT-23-IP-026. Slovenian Research Agency for co-financing of this work through the Research Programme P4-0015 and project J7-50231-Growth.

Author contributions: Dabosmita Paul: writing – review and editing, writing – original draft, visualisation, methodology, investigation, formal analysis, data curation, conceptualisation. Marko Petrič: writing – review and editing, writing – original draft, validation, formal analysis, conceptualisation. Miha Humar: writing – review and editing, visualization, validation. Erika Švara Fabjan: writing – review and editing, validation, data curation.

Milan Gaff: writing – review and editing, validation. Daniela Tesařová: writing – review and editing, validation, investigation, conceptualisation. All authors have accepted responsibility for the entire content of this manuscript and approved its submission.

Conflict of interest: The authors state no conflict of interest.

Data availability statement: The datasets generated and/or analysed during the current study are available from the corresponding author on reasonable request.

References

[1] Feist W, Hon D. Chemistry of weathering and protection. In The chemistry of solid wood. 1984. p. 207, 401–51.

[2] Rowell R, ed. The chemistry of solid wood. In Advances in chemistry. Vol. 207. Washington, DC: American Chemical Society; 1984. doi: 10.1021/ba-1984-0207.

[3] Rowell RM, Rowell RM, Eds. Handbook of wood chemistry and wood composites. Boca Raton: CRC Press; 2005. doi: 10.1201/9780203492437.

[4] Stamm AJ. Wood and cellulose science.

[5] Hill CA. Wood modification: Chemical, thermal and other processes. Chichester, UK: John Wiley & Sons; 2007.

[6] Chang H-T, Chang S-T. Moisture excluding efficiency and dimensional stability of wood improved by acylation. Bioresour Technol. 2002;2(85):201–4.

[7] Han X, Wang Z, Zhang Q, Pu J. An effective technique for constructing wood composite with superior dimensional stability. Holzforschung. May 2020;74(5):435–43. doi: 10.1515/hf-2019-0176.

[8] Rowell RM, Banks WB. Water repellency and dimensional stability of wood, Gen. Tech. Rep. FPL-50. Vol. 50. Madison, WI: US Department of Agriculture, Forest Service, Forest Products Laboratory; 1985. p. 24.

[9] Fathi H, Kazemirad S, Nasir V. Mechanical degradation of wood under ultraviolet radiation characterized by Lamb wave propagation. Struct Control Health Monit. Jun. 2021;28(6):e2731. doi: 10.1002/stc.2731.

[10] Bi Z, Zhou X, Chen J, Lei Y, Yan L. Effects of extracts on color, dimensional stability, and decay resistance of thermally modified wood. Eur J Wood Prod. Apr. 2024;82(2):387–401. doi: 10.1007/s00107-023-02024-4.

[11] Vek V, Balzano A, Poljanšek I, Humar M, Oven P. Improving fungal decay resistance of less durable sapwood by impregnation with scots pine knotwood and black locust heartwood hydrophilic extractives with antifungal or antioxidant properties. Forests. Sep. 2020;11(9). Art. no. 9. doi: 10.3390/f11091024.

[12] Bi W, Li H, Hui D, Gaff M, Lorenzo R, Corbi I, et al. Effects of chemical modification and nanotechnology on wood properties. Nanotechnol Rev. Aug. 2021;10(1):978–1008. doi: 10.1515/ntrev-2021-0065.

[13] Chujo Y. Organic—inorganic hybrid materials. Curr Opin Solid State Mater Sci. Dec. 1996;1(6):806–11. doi: 10.1016/S1359-0286(96)80105-7.

[14] Wight AP, Davis ME. Design and preparation of organic-inorganic hybrid catalysts. Chem Rev. 2002;102(10):3589–614. doi: 10.1021/cr010334m.

[15] Merk V, Chanana M, Keplinger T, Gaan S, Burgert I. Hybrid wood materials with improved fire retardance by bio-inspired mineralisation on the nano- and submicron level. Green Chem. 2015;17(3):1423–8. doi: 10.1039/c4gc01862a.

[16] Lou Z, Han H, Zhou M, Han J, Cai J, Huang C, et al. Synthesis of magnetic wood with excellent and tunable electromagnetic wave-absorbing properties by a facile vacuum/pressure impregnation method. ACS Sustain Chem Eng. Jan. 2018;6(1):1000–8. doi: 10.1021/acssuschemeng.7b03332.

[17] Oka H, Hojo A, Osada H, Namizaki Y, Taniuchi H. Manufacturing methods and magnetic characteristics of magnetic wood. J Magn Magn Mater. May 2004;272–276:2332–4. doi: 10.1016/j.jmmm.2003.12.1214.

[18] Iqbal J, Safdar N, Jan T, Ismail M, Hussain SS, Mahmood A, et al. Facile synthesis as well as structural, Raman, dielectric and antibacterial characteristics of Cu doped ZnO nanoparticles. J Mater Sci Technol. Mar. 2015;31(3):300–4. doi: 10.1016/j.jmst.2014.06.013.

[19] Mantanis G, Terzi E, Kartal SN, Papadopoulos AN. Evaluation of mold, decay and termite resistance of pine wood treated with zinc- and copper-based nanocompounds. Int Biodeterior Biodegrad. May 2014;90:140–4. doi: 10.1016/j.ibiod.2014.02.010.

[20] Sun Q, Lu Y, Yang D, Li J, Liu Y. Preliminary observations of hydrothermal growth of nanomaterials on wood surfaces. Wood Sci Technol. Jan. 2014;48(1):51–8. doi: 10.1007/s00226-013-0570-7.

[21] de Maria VP, de Paiva FF, Tamashiro JR, Silva LH, da Silva Pinho G, Rubio-Marcos F, et al. Advances in ZnO nanoparticles in building material: Antimicrobial and photocatalytic applications–Systematic literature review. Constr Build Mater. 2024;417:135337.

[22] Venkatesh N, Aravindan S, Ramki K, Murugadoss G, Thangamuthu R, Sakthivel P. Sunlight-driven enhanced photocatalytic activity of bandgap narrowing Sn-doped ZnO nanoparticles. Environ Sci Pollut Res. 2021;28(13):16792–803. doi: 10.1007/s11356-020-11763-3.

[23] Lemaire-Paul M, Beuthe CA, Riahinezhad M, Reza Foruzanmehr M. The impact of vacuum pressure on the effectiveness of SiO_2 impregnation of spruce wood. Wood Sci Technol. Jan. 2023;57(1):147–71. doi: 10.1007/s00226-022-01448-0.

[24] Singh R, Kumar S. Regulatory and safety concerns regarding the use of active nanomaterials in food industry. In Nanotechnology advancement in agro-food industry. Singapore: Springer Nature Singapore; 2023. p. 269–306. doi: 10.1007/978-981-99-5045-4_8.

[25] Liao C-M, Chiang Y-H, Chio C-P. Assessing the airborne titanium dioxide nanoparticle-related exposure hazard at workplace. J Hazard Mater. Feb. 2009;162(1):57–65. doi: 10.1016/j.jhazmat.2008.05.020.

[26] Wang B, Feng M, Zhan H. Improvement of wood properties by impregnation with TiO_2 via ultrasonic-assisted sol–gel process. RSC Adv. 2014;4(99):56355–60.

[27] Úradníček L, Madera P, Koblížek J, Tichá S. Dřeviny České republiky. 2009.

[28] Raspor P, Smole-Možina S, Podjavoršek J, Pohleven F, Gogala N, Nekrep FV, et al. ZIM: Collection of industrial microorganisms. Catalogue of cultures. Ljubljana: University of Ljubljana, Biotechnical Faculty; 1995. p. 98.

[29] Carey JK, Bravery AF. A technique for assessing the preventative efficacy against decay fungi of preservative treatments applied to wood. Int Biodeterior. 1989;25(6):439–44.

[30] Wang X, Chai Y, Liu J. Formation of highly hydrophobic wood surfaces using silica nanoparticles modified with long-chain alkylsilane. Holzforschung. Aug. 2013;67(6):667–72. doi: 10.1515/hf-2012-0153.
[31] Weichelt F, Emmler R, Flyunt R, Beyer E, Buchmeiser MR, Beyer M. ZnO-based UV nanocomposites for wood coatings in outdoor applications. Macromol Mater Eng. 2010;295(2):130–6. doi: 10.1002/mame.200900135.
[32] Goldstein JI, Newbury DE, Michael JR, Ritchie NWM, Scott JHJ, Joy DC. Scanning electron microscopy and X-ray microanalysis. Switzerland: Springer; 2017.
[33] Yao Q, Wang C, Fan B, Wang H, Sun Q, Jin C, et al. One-step solvothermal deposition of ZnO nanorod arrays on a wood surface for robust superamphiphobic performance and superior ultraviolet resistance. Sci Rep. Oct. 2016;6(1):35505. doi: 10.1038/srep35505.
[34] Carrillo I, Mendonça RT, Ago M, Rojas OJ. Comparative study of cellulosic components isolated from different Eucalyptus species. Cellulose. Feb. 2018;25(2):1011–29. doi: 10.1007/s10570-018-1653-2.
[35] Popescu C-M, Popescu M-C, Singurel G, Vasile C, Argyropoulos DS, Willfor S. Spectral characterization of eucalyptus wood. Appl Spectrosc. Nov. 2007;61(11):1168–77. doi: 10.1366/000370207782597076.
[36] Dong Y, Yan Y, Ma H, Zhang S, Li J, Xia C, et al. In situ chemosynthesis of ZnO nanoparticles to endow wood with antibacterial and UV-resistance properties. J Mater Sci Technol. Mar. 2017;33(3):266–70. doi: 10.1016/j.jmst.2016.03.018.
[37] Urbano M, Paez J. Amorphous TiO_2 nanoparticles: Synthesis and antibacterial capacity. J Non-Cryst Solids. Mar. 2017;459:192–205. doi: 10.1016/j.jnoncrysol.2017.01.018.
[38] Liu QX, Xu WC. Study on amorphous silica powder properties. Adv Mater Res. 2012;512–515:2428–33. doi: 10.4028/www.scientific.net/AMR.512-515.2428.
[39] Kirkbride KP. Analytical techniques | Spectroscopic techniques. In: Siegel JA, editor. In Encyclopedia of forensic sciences. Oxford: Elsevier; 2000. p. 179–91. doi: 10.1006/rwfs.2000.0790.
[40] Gan W, Gao L, Sun Q, Jin C, Lu Y, Li J. Multifunctional wood materials with magnetic, superhydrophobic and anti-ultraviolet properties. Appl Surf Sci. Mar. 2015;332:565–72. doi: 10.1016/j.apsusc.2015.01.206.
[41] Zheng R, Tshabalala MA, Li Q, Wang H. Construction of hydrophobic wood surfaces by room temperature deposition of rutile (TiO_2) nanostructures. Appl Surf Sci. Feb. 2015;328:453–8. doi: 10.1016/j.apsusc.2014.12.083.
[42] Wang B, Feng M, Zhan H. Improvement of wood properties by impregnation with TiO_2 via ultrasonic-assisted sol–gel process. RSC Adv. Oct. 2014;4(99):56355–60. doi: 10.1039/C4RA04852K.
[43] Wang S, Liu C, Liu G, Zhang M, Li J, Wang C. Fabrication of superhydrophobic wood surface by a sol–gel process. Appl Surf Sci. Nov. 2011;258(2):806–10. doi: 10.1016/j.apsusc.2011.08.100.
[44] Yin H, Moghaddam MS, Tuominen M, Dėdinaitė A, Wålinder M, Swerin A. Wettability performance and physicochemical properties of UV exposed superhydrophobized birch wood. Appl Surf Sci. May 2022;584:152528. doi: 10.1016/j.apsusc.2022.152528.
[45] Nagraik P, Shukla SR, Kelkar BU, Paul BN. Wood modification with nanoparticles fortified polymeric resins for producing nano-wood composites: a review. J Indian Acad Wood Sci. Jun. 2023;20(1):1–11. doi: 10.1007/s13196-023-00313-2.
[46] Jiang J, Cao J, Wang W. Characteristics of wood-silica composites influenced by the pH value of silica sols. Holzforschung. Apr. 2018;72(4):311–9. doi: 10.1515/hf-2017-0126.
[47] Xu B, Zhang Q. Preparation and properties of hydrophobically modified nano-SiO_2 with hexadecyltrimethoxysilane. ACS Omega. Apr. 2021;6(14):9764–70. doi: 10.1021/acsomega.1c00381.
[48] Mardosaitė R, Jurkevičiūtė A, Račkauskas S. Superhydrophobic ZnO nanowires: Wettability mechanisms and functional applications. Cryst Growth Des. Aug. 2021;21(8):4765–79. doi: 10.1021/acs.cgd.1c00449.
[49] Wang B, Feng M, Zhan H. Improvement of wood properties by impregnation with TiO 2 via ultrasonic-assisted sol–gel process. RSC Adv. 2014;4(99):56355–60.
[50] Dong Y, Yan Y, Zhang S, Li J, Wang J. Flammability and physical–mechanical properties assessment of wood treated with furfuryl alcohol and nano-SiO_2. Eur J Wood Prod. Jul. 2015;73(4):457–64. doi: 10.1007/s00107-015-0896-y.
[51] Xing D, Zhang Y, Hu J, Yao L. Highly hydrophobic and self-cleaning heat-treated Larix spp. prepared by TiO_2 and ZnO particles onto wood surface. Coatings. Oct. 2020;10(10):Art. no. 10. doi: 10.3390/coatings10100986.
[52] Li J, Sun Q, Yao Q, Wang J, Han S, Jin C. Fabrication of robust superhydrophobic bamboo based on ZnO nanosheet networks with improved water-, UV-, and fire-resistant properties. J Nanomater. 2015;2015:431426. doi: 10.1155/2015/431426.
[53] Rassam G, Abdi Y, Abdi A. Deposition of TiO_2 nano-particles on wood surfaces for UV and moisture protection. J Exp Nanosci. Jul. 2012;7(4):468–76. doi: 10.1080/17458080.2010.538086.
[54] Temiz A, Terziev N, Eikenes M, Hafren J. Effect of accelerated weathering on surface chemistry of modified wood. Appl Surf Sci. 2007;253(12):5355–62.
[55] Cogulet A, Blanchet P, Landry V. Wood degradation under UV irradiation: A lignin characterization. J Photochem Photobiol B: Biol. Mar. 2016;158:184–91. doi: 10.1016/j.jphotobiol.2016.02.030.
[56] Geffertova J, Geffert A, Vybohova E. The effect of UV irradiation on the colour change of the spruce wood. Acta Fac Xylolog. Jan. 2018;60:41–50. doi: 10.17423/afx.2018.60.1.05.
[57] Mai C, Militz H. Modification of wood with silicon compounds. Treatment systems based on organic silicon compounds - A review. Wood Sci Technol. Apr. 2004;37:453–61. doi: 10.1007/s00226-004-0225-9.
[58] Liu B, Tang J, Li J, Shan Y, Jiang Y. Soft wetting: Modified Cassie-Baxter equation for soft superhydrophobic surfaces. Colloids Surf A: Physicochem Eng Asp. 2023;677:132348.
[59] Mohammed MM, Rasidi M, Mohammed AM, Rahman RB, Osman AF, Adam T, et al. Interfacial bonding mechanisms of natural fibre-matrix composites: An overview. BioResources. Aug. 2022;17:7031. doi: 10.15376/biores.17.4.Mohammed.
[60] Gao L, Lu Y, Zhan X, Li J, Sun Q. A robust, anti-acid, and high-temperature–humidity-resistant superhydrophobic surface of wood based on a modified TiO2 film by fluoroalkyl silane. Surf Coat Technol. Jan. 2015;262:33–9. doi: 10.1016/j.surfcoat.2014.12.005.
[61] Seo K, Kim M, Kim DH, Seo K, Kim M, Kim DH. Re-derivation of Young's equation, Wenzel equation, and Cassie-Baxter equation based on energy minimization. Surf Energy. IntechOpen; 2015. p. 1–19. doi: 10.5772/61066.
[62] Reinprecht L, Repák M, Iždinskỳ J, Vidholdová Z. Decay resistance of nano-zinc oxide, and PEG 6000, and thermally modified wood. Forests. 2022;13(5):731.
[63] European Standard. 2016. EN 350. Durability of wood and wood-based products - Testing and classification of the durability to biological agents of wood and wood-based materials.
[64] Bolton AJ, Petty JA. Variation of susceptibility to aspiration of bordered pits in conifer wood. J Exp Bot. Aug. 1977;28(4):935–41. doi: 10.1093/jxb/28.4.935.
[65] Richardson BA. Wood preservation. London: E. & F.N. Spon, 1993.